VIP Heterogeneous Catalysis

DOI: 10.1002/anie.201300538

Synergy between XANES Spectroscopy and DFT to Elucidate the Amorphous Structure of Heterogeneous Catalysts: TiO_2-Supported Molybdenum Oxide Catalysts**

*Asma Tougerti, Elise Berrier, Anne-Sophie Mamede, Camille La Fontaine, Valérie Briois, Yves Joly, Edmond Payen, Jean-François Paul, and Sylvain Cristol**

The properties of heterogeneous catalysts are directly correlated to the molecular structure of the active sites which often consists of nanometer-scale particles of transition metals (in a metallic, oxide or sulfide form) dispersed on an oxide support.[1] The complexity of physico-chemical phenomena occurring during the catalyst synthesis/activation stages often leads to the formation of unknown supported phases featuring new ill-defined sites.[2] Their identification requires an in-depth characterization at the molecular scale of the catalyst with the use of various spectroscopic tools. Despite the valuable information so-obtained, these techniques sometimes are not able to provide the overall structure of the active species responsible for the catalytic activity. The use of theoretical tools to establish direct correlation between spectroscopic fingerprints and structural/electronic properties of catalysts is a powerful and quite new approach for unraveling the structure of catalysts.

Thanks to its chemical and electronic (orbital) selectivity, X-ray absorption near-edge structure (XANES) spectroscopy is the technique of choice for molecular-scale characterization of catalysts. Furthermore, in the XANES spectra, the long mean free path of the photoelectron, induced by its small kinetic energy ($E_c < 50$–100 eV), provides a high contribution of multiple scattering events of the photoelectron allowing to probe the three-dimensional structure (3D) around the absorbing atom.[3] XANES spectroscopy is however highly dependent on electronic parameters that make its fine interpretation difficult. This often leads to a restricted use of XANES spectra for the determination of the oxidation state of an absorber atom or/and basic consideration on its local symmetry. It is however possible to obtain a finer interpretation of spectra by calculation of XANES transitions. Indeed, the multiple scattering (MS) theory is well adapted to reproduce the XANES transitions observed at K edges of elements heavier than Li and at $L_{2,3}$ edges of elements heavier than Cd.[3]

We propose herein to use MS simulations based on structural models predicted by DFT calculations for interpreting the Mo_K edge fingerprints observed for TiO_2-supported molybdenum oxide catalysts which are widely used for olefin metathesis,[4] selective oxidation reactions,[5] and hydrotreatment.[6] The structure of the oxomolybdate species formed during the catalyst activation is still unknown even though it has been extensively characterized by various spectroscopies.[7] A three-step methodology was followed to unravel the catalyst structure: first simulations of XANES spectra of Mo reference compounds (ammonium heptamolybdate (hereafter noted AHM), $(NH_4)_3[Al(OH)_6Mo_6O_{18}]$ (noted $AlMo_6$), α-$(NH_4)_4[Mo_8O_{26}]$ (noted Mo_8O_{26})) were performed to obtain direct correlation between spectroscopic fingerprints and structural properties of known structures. Then, these fingerprints are identified in the spectrum of the supported catalyst to generate catalyst structures for DFT optimization. Finally, the optimized geometry is used for modeling XANES spectra using MS theory.

Figure 1 A presents Mo_K edge experimental spectra of the activated catalyst (350 °C in oxygen), labeled hereafter 7.5 MoTi, together with four reference compounds in which

[*] Dr. A. Tougerti, Dr. E. Berrier, Dr. A.-S. Mamede, Prof. E. Payen, Prof. J.-F. Paul, Prof. S. Cristol
Université Lille 1
Unité de Catalyse et de Chimie du Solide, UMR CNRS 8181
59655 Villeneuve d'Ascq Cedex (France)
E-mail: sylvain.cristol@univ-lille1.fr
Dr. C. La Fontaine, Dr. V. Briois
Synchrotron Soleil
Gif-sur-Yvette (France)
Dr. Y. Joly
Institut Néel, CNRS-Université J. Fourier
Grenoble (France)

[**] We wish to acknowledge the Agence Nationale de la Recherche for funding under the contract number ANR-07-BLAN-0265-01 (Spectroscopie d'Absorption X Operando). XANES = X-ray absorption near-edge structure.

Supporting information for this article is available on the WWW under http://dx.doi.org/10.1002/anie.201300538.

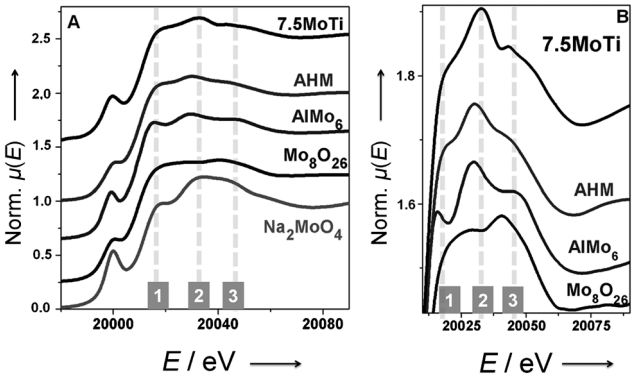

Figure 1. A) Mo_K edge XANES spectra of model compounds and the 7.5 MoTi catalyst (Norm. $\mu(E)$ = normalized absorption). B) Zoom on Mo_K edge XANES spectra for octahedral model compounds and the 7.5 MoTi catalyst at 75 eV beyond the pre-edge.

molybdenum is either located in four-fold coordinated sites (Na_2MoO_4) or in six-fold coordinated sites (AHM, $AlMo_6$, and Mo_8O_{26}). The dissimilarity of both pre-edge intensity and global spectrum shape between Na_2MoO_4 and Mo-supported catalyst rules out a tetrahedral symmetry for the Mo atoms of the catalysts. Conversely, the XANES spectrum of the catalyst exhibits similar characteristics of polyoxoanions compounds (Figure 1 A). This indicates that the supported phase contains octahedral polymeric Mo. Although the spectra of six-fold coordinated Mo sites are very similar, a careful inspection in the region around 75 eV beyond the absorption edge (Figure 1 B) shows that it is possible to distinguish two octahedral polymeric Mo structures. For AHM and $AlMo_6$ compounds, the spectra display three successive features at about 20017, 20030, and 20047 eV (denoted as 1, 2, and 3 in Figure 1 B) whereas the Mo_8O_{26} spectrum only shows two features at about 20017 and 20042 eV. It is also possible to get a more acute characterization of the specific intensity of the second bump by comparing the amplitude of absorption between the first and the second bump. The second bump has a significantly higher relative intensity in the spectrum of $AlMo_6$ compared to the one observed in the XANES spectrum of AHM. To understand the origin of these bumps XANES simulation of Mo polyoxoanion compounds has been carried out.

Experimental and calculated XANES spectra of AHM are shown in Figure 2 C along with a schematic structural representation of the polyoxoanion (Figure 2 A). The AHM structure is made of edge-sharing distorted octahedra featuring two short adjacent terminal Mo=O_t bonds and four Mo–O distances ranging from 1.9 to 2.4 Å. The AHM compound has three non-equivalent Mo sites (Figure 2 A) which will be further denoted 1, 1′, and 2. Sites 1 and 1′ are both characteristic of a Mo atom surrounded by three Mo neighbors. The differences between sites 1 and 1′ are a longer Mo–O bond (2.4 instead of 2.3 Å) and different ∡ OMoO angles. Site 2 Mo is surrounded by six Mo atoms with a spread in Mo–O distances similar to that of site 1. The XANES spectra calculation was performed considering all non-equivalent Mo sites (1, 1′, and 2). The calculated spectra were then summed using the relative weight of each site in the AHM structure to get the final overall spectrum. The obtained spectrum is lastly convoluted before it is compared with the experimental spectrum.

The XANES contributions of each Mo site (1, 1′, and 2) calculated using clusters of five different radii are reported in Figure 2 D, E, and F. For a cluster radius equal to 2.5 Å (which corresponds to one Mo atom and six surrounding oxygen atoms; Figure 2 B, $R = 2.5$ Å), only site 1′ presents an intense third bump. The comparison of the calculated overall final spectrum to the experimental one (Figure 2 C, $R = 2.5$ Å), shows however that the shapes of the bumps are not well reproduced by the calculation.

The increase of the calculated radius from the first to the second nearest shell (molybdenum) is presented in Figure 2 B ($R = 3.3$ Å) and does not show significant changes compared to the smaller calculated radius.

The addition of a second oxygen coordination shell (Figure 2 B, $R = 4$ Å) gives rise to more pronounced spectral features in the calculated individual contributions (Figure 2 D, E, F, $R = 4$ Å). Furthermore, the calculated overall final spectrum well reproduces the experimental spectrum, especially the shape and the intensity of the bumps (Figure 2 C, $R = 4$ Å). This is a clear indication that the second oxygen coordination shell belonging to the neighboring octahedra and standing between 3.3 and 4 Å is responsible for the typical XANES profile of AHM. Note also the peculiar spectral shape of the individual XANES of the site 2 Mo

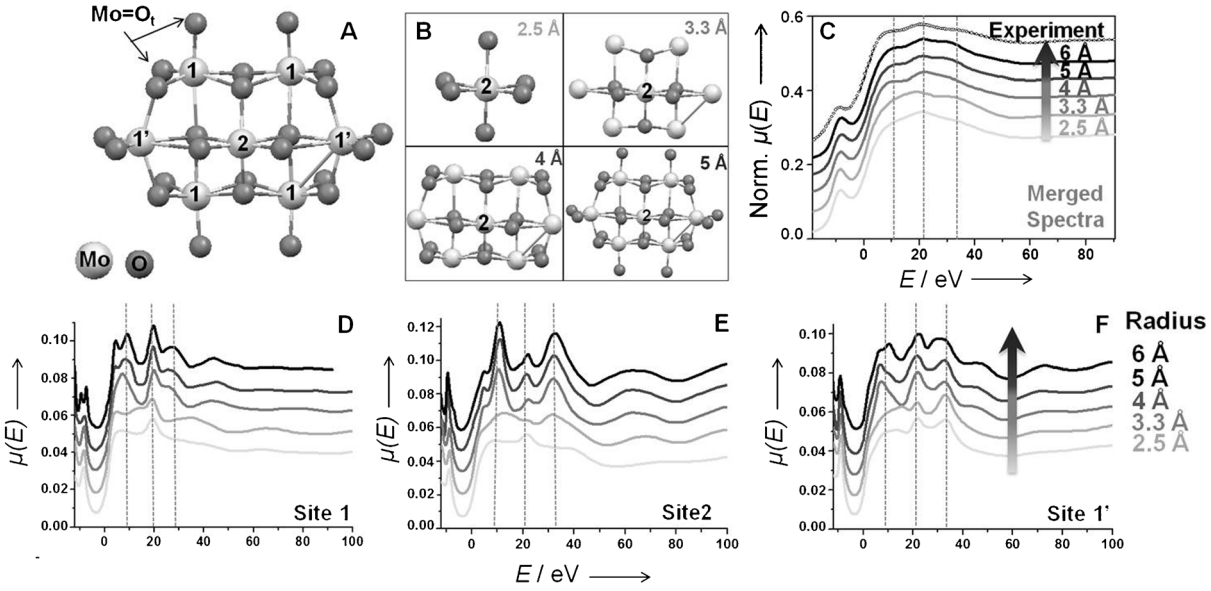

Figure 2. A) Structure of AHM. B) Shells around site 2 Mo for cluster radii equal to 2.5, 3.3, 4, and 5 Å. C) Normalized (with respect to the experimental spectrum) theoretical Mo_K edge XANES spectra of AHM at five different cluster radii together with the experimental spectrum. D, E and F) Non-convoluted calculated Mo_K edge XANES spectra of sites 1, 2, and 1′ Mo, respectively, at five different radii for the AHM cluster.

(Figure 2E, $R = 4$ Å) which shows higher intensities of both the first and third bumps and a much less intense second bump relative to that of sites 1 (Figure 2D, $R = 4$ Å) and 1′ (Figure 2F, $R = 4$ Å). This is due to the specific second oxygen shell of site 2 Mo in comparison to sites 1 and 1′ (Figure 2A). It is well reported that scattering amplitudes of low-Z elements are strongly peaked near the Fermi energy and rapidly decreases when increasing the energy making XANES sensitive to low-Z elements.[8] Finally, the calculations at higher cluster radii (5 and 6 Å) demonstrate that convergence is reached at 5 Å.

The intensity ratio of resonances characterizing the experimental XANES spectrum of AHM is fixed by the specific surrounding environment (oxygen atoms) of each non-equivalent Mo site forming the polyoxoanion. Similar findings arise from calculated XANES spectra of $AlMo_6$ and Mo_8O_{26} compounds (Figure 3). All six Mo atoms of the $AlMo_6$ structure are surrounded by two molybdenum and one

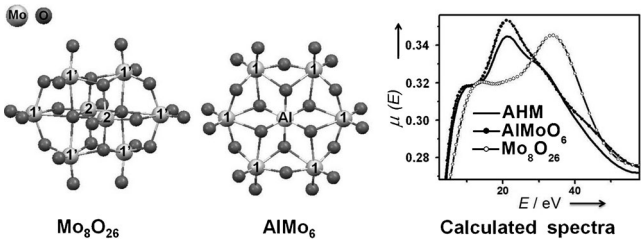

Figure 3. Structures of Mo_8O_{26} and $AlMo_6$ with calculated Mo K-edge XANES spectra of AHM, Mo_8O_{26}, and $AlMo_6$.

aluminum atoms; they present a local environment, especially a second coordination shell of oxygen atoms, quite similar to those of site 1 Mo in AHM. However, the absence of site 2 Mo (site 2 shows high intensities of both the first and third bumps and a very low intensity of the second bump) favors a second bump of higher relative intensity for $AlMo_6$ relative to the one obtained for AHM. For Mo_8O_{26}, the contribution of site 2 Mo in the overall calculated intensity of the spectrum is twice higher than that in AHM. This feature added to the existence of site 1′ Mo (giving rise to a high intense third bump relative to site 1 Mo), leads to the absence of a well-defined structure of the second bump and the presence of an intense third bump.

From the data discussed above it can be stated that the intensity of the second bump in the Mo_K edge XANES spectrum is a good spectral fingerprint of the presence/absence of site 2 Mo. The 7.5 MoTi catalyst shows a second bump of an intensity similar to the one of $AlMo_6$ (Figure 1B). Thus, it can be concluded that the active phase of the Mo catalyst is characterized by the absence of site 2 Mo. Following this hypothesis, a relevant candidate for a structural model of the active phase of the catalyst could be a six-membered ring formed by Mo atoms in octahedral symmetry without site 2 Mo. We studied the adsorption of this potential active phase on a TiO_2 surface by DFT optimization. The anatase support was modeled by the mainly exposed (101) surface.[9]

In addition to the six-membered ring structures, other potential active phases structures showing Mo atoms in octahedral symmetry without site 2 Mo are also plausible, such as infinite chain structures and trimeric/tetrameric clusters (see Section S1 in the Supporting Information). However, DFT calculations show that such structures are unstable on a TiO_2 surface and strongly reconstructed losing their octahedral symmetry after geometry optimization and lead to a very bad agreement between experiment and theory (see Section S2 in the Supporting Information).

Conversely, the octahedral symmetry of the ring structure (the chemical formula is $[Mo_6O_{21}]^{6-}$) is preserved after DFT relaxation. Such a structure however gives rise to discrepancies between experiment and theory that can be explained by the small size of the $Mo_6O_{21}{}^{6-}$ cluster showing highly distorted octahedra at the edge of the structure. To overcome this edge effect while keeping the ring structure, Mo_4O_{12} entities (Figure 4) were added to the $Mo_6O_{21}{}^{6-}$ structure. This induces a decrease of the contribution of the edge molybdenum and gives rise to a more consistent simulated XANES spectrum. In fact, the $[Mo_6O_{21}(Mo_4O_{12})_2]^{6-}$ structure (Figure 4) leads to a good reproduction of the intensity of the second bump which is in line with the absence of site 2 Mo. Moreover, the adsorption of the $[Mo_6O_{21}(Mo_4O_{12})_2]^{6-}$ structure is, in contrast to clusters and chain structures, exothermic (−0.7 eV, see Section S3 in the Supporting Information).

Further increase of the $[Mo_6O_{21}(Mo_4O_{12})_2]^{6-}$ cluster size by successive addition of Mo_4O_{12} entities can also be done without significant alteration of the calculated XANES spectrum. Indeed increasing the cluster size will increase the intensity of the second shoulder until a critical cluster size is reached for which the Mo atoms located at the edge will have a minimal influence on the total spectrum. This prevents any further attempt to fully determine the mean size of the cluster using DFT and XANES spectroscopy. Nevertheless, we can reliably propose that the configuration of the catalyst surface after activation is $[Mo_{14}O_{45}(Mo_4O_{12})_n]^{6-}$ where $n \geq 2$ is the number of Mo_4O_{12} cluster(s) added for increasing the cluster size of the polyanion. This is in agreement with previous conclusions drawn by Raman spectroscopy showing that oxide Mo species adsorbed on a TiO_2 surface are in a polymeric form possessing only one terminal Mo=O bond.[7] The relevance of the $[Mo_6O_{21}(Mo_4O_{12})_2]^{6-}$ structure is also clearly shown by the calculation of the theoretical extended X-ray absorption fine structure (EXAFS) spectrum where every experimental EXAFS oscillation is well reproduced (Figure 4).

After a calcination step the structure of TiO_2-supported oxomolybdates does not depend on the preparation method.[11] This strongly suggests that the supported phase is obtained under thermodynamic control which is in line with the findings of this work. Indeed, molybdenum species forming the $[Mo_6O_{21}(Mo_4O_{12})_2]^{6-}$ are almost in epitaxial interaction with the TiO_2 (101) surface (Figure 4) and show the classical molybdenum linking mode observed either in MoO_3 crystals and AHM. This demonstrates the prominent influence of the support on the structure of the active phase of the Mo-supported catalyst as the speciation of supported Mo atoms is not only fixed by the Mo chemistry but also by the

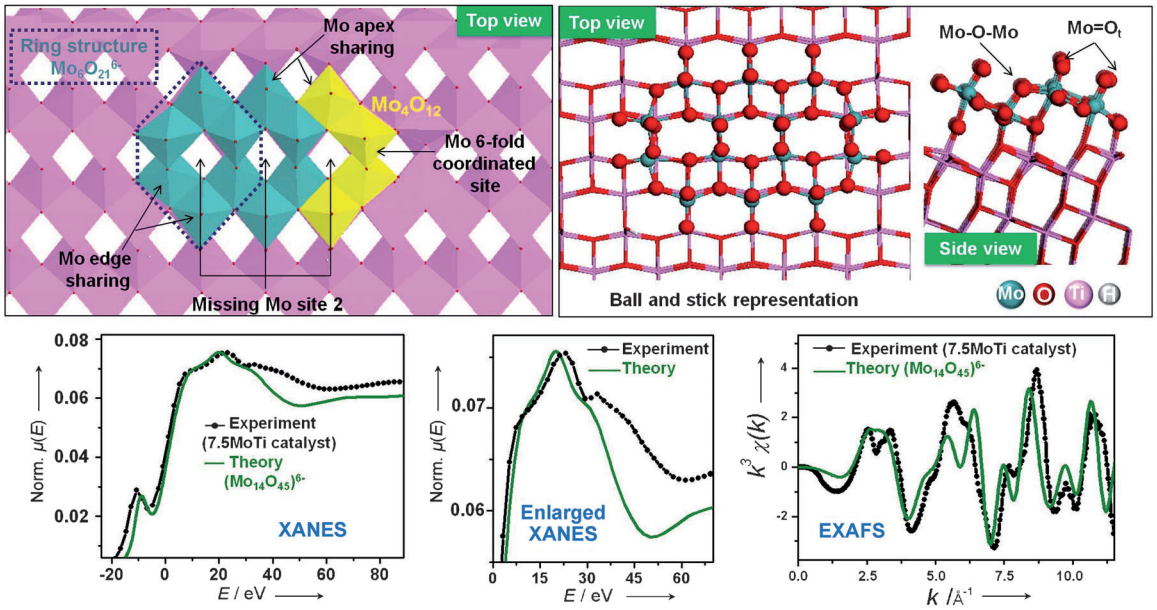

Figure 4. Ring Mo structure on the (101) TiO_2 surface along with calculated (green line) and experimental (dark line) XANES and EXAFS spectra of the 7.5 MoTi catalyst. The theoretical EXAFS spectrum is obtained by summing the scattering paths which are achieved by the calculation of the scattering amplitude, phase functions, and mean free paths.

structure of the TiO_2 surface which imposes the arrangement of the Mo octahedra.

In summary, the combination of XANES spectroscopy, DFT, and MS simulations can be very powerful for solving the structure of heterogeneous catalysts. This approach has a general interest much broader than catalysis, as it can be straightforwardly extended to other relevant systems were conventional diffraction techniques cannot be applied such as the large class of nanostructured materials.

Experimental Section

A TiO_2-supported molybdenum oxide catalyst was prepared by impregnation of anatase TiO_2 powder (BET surface equal to 93 $m^2 g^{-1}$) by an aqueous solution of AHM, the concentration of which was adjusted to reach a final composition of 7.5 %wt MoO_3/TiO_2 (7.5 MoTi). The catalyst was then calcined 6 h at 400 °C in pure oxygen.

The XAS spectra were recorded at SOLEIL synchrotron facility on the SAMBA beamline.[12] In Section S4 of the Supporting Information, further details on the temperature/gas flow used during recording the spectra are available.

The computational details are given in Section S5 in the Supporting Information. Briefly, the ab initio simulations of the XANES spectra have been performed using the FDMNES package (Section S5.1 in the Supporting Information).[3] DFT calculations, in the framework of the GGA-PBE functional,[13] were performed with the VASP code (Section S5.2 in the Supporting Information).[13]

Received: January 21, 2013
Revised: April 11, 2013
Published online: May 7, 2013

Keywords: ab initio calculations · heterogeneous catalysis · molybdenum · X-ray absorption spectroscopy

[1] J. A. Dumesic, G. W. Huber, M. Boudart in *Handbook of Heterogeneous Catalysis* (Eds.: G. Ertl, H. Knözinger, F. Schüth, J. Weitkamp), Wiley-VCH, Weinheim, **2008**, pp. 1–15.

[2] a) S. Boujday, J.-F. Lambert, M. Che, *Top. Catal.* **2003**, *24*, 37–42; b) E. Marceau, X. Carrier, M. Che, O. Clause, C. Marcilly in *Handbook of Heterogeneous Catalysis* (Eds.: G. Ertl, H. Knözinger, F. Schüth, J. Weitkamp), Wiley-VCH, Weinheim, **2008**, pp. 467–484.

[3] a) V. Briois, C. Cartier dit Moulin, P. Sainctavit, C. Brouder, A.-M. Flank, *J. Am. Chem. Soc.* **1995**, *117*, 1019–1026; b) C. R. Natoli, M. Benfatto, *J. Phys. (Paris) Colloq.* **1986**, *47*, C8–11; c) A. L. Ankudinov, B. Ravel, J. J. Rehr, S. D. Conradson, *Phys. Rev. B* **1998**, *58*, 7565–7576; d) Y. Joly, *Phys. Rev. B* **2001**, *63*, 125120; e) C. Lamberti, G. T. Palomino, S. Bordiga, G. Berlier, F. D'Acapito, A. Zecchina, *Angew. Chem.* **2000**, *112*, 2222–2225; *Angew. Chem. Int. Ed.* **2000**, *39*, 2138–2141.

[4] a) Y. Iwasawa, H. Kubo, H. Hamamura, *J. Mol. Catal.* **1985**, *28*, 191–208; b) J. L. G. Fierro, J. C. Mol in *Metal Oxides: Chemistry and Applications* (Eds.: J. L. G. Fierro), TAYLOR & FRANCIS, Boca Raton, FL, **2006**, pp. 517–554.

[5] a) H. Hu, I. E. Wachs, *J. Phys. Chem.* **1995**, *99*, 10911–10922; b) R. B. Watson, U. S. Ozkan, *J. Catal.* **2002**, *208*, 124–138.

[6] a) H. Topsøe, B. S. Clausen, F. E. Massoth in *Hydrotreating Catalysis, Science and Technology* (Eds.: J. R. Anderson, M. Boudard), Springer, Berlin, **1996**; b) J. A. Bergwerff, M. Jansen, R. G. Leliveld, T. Visser, K. P. de Jong, B. M. Weckhuysen, *J. Catal.* **2006**, *243*, 292–302.

[7] a) P. Ciambelli, D. Sannino, V. Palma, V. Vaiano, R. I. Bickley, *Appl. Catal. A* **2008**, *349*, 140–147; b) G. Tsilomelekis, A. Christodoulakis, S. Boghosian, *Catal. Today* **2007**, *127*, 139–147; c) L. E. Briand, O. P. Tkachenko, M. Guraya, I. E. Wachs, W. Grünert, *Surf. Interface Anal.* **2004**, *36*, 238–245; d) K. V. R. Chary, T. Bhaskar, G. Kishan, V. Vijayakumar, *J. Phys. Chem. B* **1998**, *102*, 3936–3940; e) H. Hu, I. E. Wachs, *J. Phys. Chem.* **1995**, *99*, 10897–10910; f) D. S. Kim, I. E. Wachs, K. Segawa, *J. Catal.* **1994**, *149*, 268–277.

[8] B. Ravel, *J. Alloys Compd.* **2005**, *401*, 118–126.

[9] a) C. Arrouvel, M. Digne, M. Breysse, H. Toulhoat, P. Raybaud, *J. Catal.* **2004**, *222*, 152 – 166; b) A. Chemseddine, T. Moritz, *Eur. J. Inorg. Chem.* **1999**, 235 – 245; c) T. Ohno, K. Sarukawa, K. Tokieda, M. Matsumura, *J. Catal.* **2001**, *203*, 82 – 86.

[10] H. R. J. Ter Veen, T Kim, I. E. Wachs, H. H. Brongersma, *Catal. Today* **2009**, *140*, 197 – 201.

[11] a) S. R. Stampfl, Y. Chen, J. A. Dumesic, C. Niu, C. G. Hill, *J. Catal.* **1987**, *105*, 445 – 454; b) T. Machej, J. Haber, A. M. Turek, I. E. Wachs, *Appl. Catal.* **1991**, *170*, 155 – 163.

[12] a) V. Briois, E. Fonda, S. Belin, L. Barthe, M. Ribbens, F. Villain, C. La Fontaine, Proceedings of UVX 2010, EDP Science, **2011**, pp. 41 – 47; b) C. La Fontaine, L. Barthe, A. Rochet, V. Briois, *Catal. Today* **2013**, *205*, 148 – 158.

[13] a) J. P. Perdew, K. Burke, M. Ernzerhof, *Phys. Rev. Lett.* **1996**, *77*, 3865 – 3868; b) VASP 4.6. Available at http://cms.mpi.univie.ac.at/vasp.

